Prospects for a bad-cavity laser using a large ion crystal

Georgy A. Kazakov,[1,*] Justin Bohnet,[2] and Thorsten Schumm[1]
[1]*Vienna University of Technology, Atominstitut, Stadionallee 2, 1020 Vienna, Austria*
[2]*National Institute of Standards and Technology, Time and Frequency Division, Boulder, Colorado 80305, USA*
(Received 4 May 2017; published 14 August 2017)

We propose to build a bad-cavity laser using forbidden transitions in large ensembles of cold ions that form a Coulomb crystal in a linear Paul trap. This laser might realize an active optical frequency standard able to serve as a local oscillator in next-generation optical clock schemes. In passive optical clocks, large ensembles of ions appear less promising, as they suffer from inhomogeneous broadening due to quadrupole interactions and micromotion-related shifts. In bad-cavity lasers, however, the radiating dipoles can synchronize and generate stable and narrow-linewidth radiation. Furthermore, for specific ions, micromotion-induced shifts can be largely suppressed by operating the ion trap at a magic frequency. We discuss the output radiation properties and perform quantitative estimations for lasing on the $^3D_2 \rightarrow {}^1S_0$ transition in $^{176}Lu^+$ ions in a spherically symmetric trap.

DOI: 10.1103/PhysRevA.96.023412

I. INTRODUCTION

Optical frequency standards are the most stable clocks to date. The most advanced implementations reach a short-term stability at the $3.4 \times 10^{-16}/\sqrt{\tau}$ level [1], and systematic uncertainty of 3.2×10^{-18} [2]. Further improvement of optical frequency standards would allow a multitude of new applications in fundamental and applied science, such as the study of fundamental constant variations [3] and relativistic geodesy [4]. Modern optical clocks are *passive clocks*, where the frequency of a *local oscillator*, i.e., some stable narrow-band laser, is feedback-stabilized to a narrow *clock transition* in trapped atoms or ions, whose frequency is robust with respect to fluctuations of the environmental parameters. This clock transition may be extremely narrow, down to a nanohertz level in some species [2], but the real spectroscopic linewidth is limited by the short-term stability of the local oscillator and usually does not surpass the subhertz level. Also, on a time scale shorter than the interrogation time of the clock transition, the stability of the local oscillator entirely determines the stability of the whole frequency standard. Fluctuations of the local oscillator frequency may also contribute to the instability of the frequency standard on longer time scales via the Dick effect [5]. Therefore, improving the local oscillators is one of the key tasks for the development of more precise optical clocks. The best modern local oscillators are lasers that are prestabilized to an ultrastable macroscopic cavity. Their stability is usually limited by mechanical and thermal noise [6] and may attain a level of 8×10^{-17} on a time scale up to 1×10^3 s at room temperature [7], and even 4×10^{-17} on a time scale up to 1×10^2 s in cryogenic environments [8], but the progress in this direction is slow.

One possible alternative approach is to create an *active optical frequency standard*, i.e., a laser where atoms with a narrow and robust lasing transition play the role of the gain medium. Such a laser would operate in the so-called bad-cavity regime, where the linewidth of the cavity mode is much broader than the gain profile. The output frequency of such a laser is determined primarily by the gain medium, which makes it robust to fluctuations of the cavity length. Such standards have been proposed by several authors recently [9–11], and a series of proof-of-principle experiments has been performed [12–16].

Active atoms that constitute the gain for an active optical frequency standard must be confined to the Lamb-Dicke regime to avoid Doppler and recoil shifts. Such a confinement may be realized with an optical lattice potential at a so-called magic frequency, where the upper and the lower lasing states experience the same ac Stark shift [17]. These shifts depend on the polarization of the trapping fields and can be controlled to the necessary level of precision only for $^3P_0 \rightarrow {}^1S_0$ transitions in Sr and other alkaline-earth-metal atoms, Zn, Cd, Hg, and Yb. A first proof-of-principle experiment with such a transition in trapped Sr atoms has been recently performed in a pulsed regime [16].

The optical lattice potential trapping neutral atoms is relatively shallow, of the order of a few tens of microkelvins [17]. This leads to a short trap lifetime; therefore, some method of compensating for atom losses must be implemented to practically realize an active optical frequency standard [18,19]. The implementation of such methods is rather complicated, although certain efforts in this direction are being made [20].

In contrast to neutral atoms, charged ions may be trapped in much deeper Paul or Penning traps, which leads to much longer trap lifetimes. Trapped ions may also be cooled via co-trapped ions of another species (sympathetic cooling) [21]. A bad-cavity laser utilizing trapped ions may operate continuously over hours, or even days, without the need to compensate for ion losses. On the other hand, micromotion of the ions and their interactions with trapping fields and with each other causes shifts and inhomogeneous broadening of the clock transition; these effects are especially pronounced in large ion ensembles. Thus, ion optical clocks have been built primarily with single ions [2–4] or with few-ion ensembles [22].

Inhomogeneous broadening may be considerably reduced for ions with negative differential polarizability of the clock states in rf Paul traps at a specially chosen magic frequency of the trapping field [23]. Also, bad-cavity lasers with inhomogeneously broadened gain may produce synchronous and stable output radiation if the total *homogeneous* broadening of the lasing transition exceeds the inhomogeneous broadening

*kazakov.george@gmail.com

by at least a few times [24]. In lasers based on a three-level scheme, such a homogeneous broadening will be dominated by repumping and related incoherent dephasing and may significantly exceed the natural linewidth of the lasing transition as well as inhomogeneous broadening of this transition. It opens the possibility to build a bad-cavity laser with ions, even if inhomogeneous broadening exceeds the natural linewidth [24].

In this paper, we present a detailed discussion of the bad-cavity laser based on Coulomb crystals in Paul traps. In Sec. II we consider a generic model of a harmonic coaxial Paul trap formed by static and rf harmonic potentials, obtain general expressions for micromotion-induced Doppler and Stark shifts in a cold Coulomb crystal, and introduce the "magic" frequency, which allows one to compensate these shifts in leading order. In Sec. III we consider residual terms of the shifts, and specify the trap geometry. In Sec. IV we derive the equation for the intracavity field, taking into account standing-wave periodicity and Gaussian shape of the cavity mode. In Sec. V we present some quantitative estimations for a bad-cavity laser with trapped $^{176}Lu^{+}$ ions. In Sec. VI we discuss the results, envisaged difficulties, and possible ways to overcome them.

II. MAGIC FREQUENCY

Here we consider micromotion-induced second-order Doppler and dc Stark shifts for ions forming a cold Coulomb crystal in a harmonic rf Paul trap. Such a many-ion crystal was considered in Ref. [23], although some higher-order terms have been omitted there. These terms, however, can be easily calculated if we note that the only macroscopic force acting on the ion in the Paul trap is proportional to the same local electric field that causes the Stark shift.

We consider a Paul trap formed by the potential

$$\phi(\bar{r},t)=\frac{m\Omega\omega_z}{2q}\,\bar{r}^{\,T}\cdot\left[\bar{\bar{\Lambda}}_{\rm rf}\cos(\Omega t)+\frac{\epsilon}{2}\bar{\bar{\Lambda}}_{\rm s}\right]\cdot\bar{r}, \tag{1}$$

where $\bar{r}=x\bar{e}_x+y\bar{e}_y+z\bar{e}_z\equiv x_1\bar{e}_x+x_2\bar{e}_y+x_3\bar{e}_z$ is the position vector, m and q are the mass and the charge of the ion, Ω is the rf drive frequency, ω_z is the frequency characterizing the trap confinement, $\epsilon=2\omega_z/\Omega$, and $\bar{\bar{\Lambda}}_{\rm rf}$ and $\bar{\bar{\Lambda}}_{\rm s}$ are traceless dimensionless symmetric matrices determining curvatures of the potentials. We use a single bar to denote column vectors with three spatial components, a double bar to denote 3×3 matrices, a dot $(\cdot)$ for the inner product, and the superscript T for the transposition (we often omit this superscript for vectors, for the sake of brevity). Also we suppose that $\omega_z\ll\Omega$, i.e., such that ϵ may be considered a small parameter.

Scaling time and length (in Gaussian units) by

$$\frac{t\Omega}{2}\to t,\quad \frac{\bar{r}}{\ell}\to\bar{r},\quad \text{where}\quad \ell=\left(\frac{q^2}{m\omega_z^2}\right)^{1/3}, \tag{2}$$

we write the equation of motion (EOM) of the ith ion as

$$\ddot{\bar{r}}_i+\epsilon^2(\bar{\bar{\Lambda}}_{\rm s}\cdot\bar{r}_i)+2\epsilon(\bar{\bar{\Lambda}}_{\rm rf}\cdot\bar{r}_i)\cos(2t)=\epsilon^2\sum_{j\neq i}\frac{\bar{r}_{ij}}{r_{ij}^3}, \tag{3}$$

where $\bar{r}_{ij}=\bar{r}_i-\bar{r}_j$, $r=|\bar{r}|$. Following Refs. [23,25] we assume the existence of a stable π-periodic solution of EOM (3), which may be expressed as

$$\bar{r}_i(t)=\bar{R}_{0,i}+2\sum_{n=1}^{\infty}\bar{R}_{2n,i}\cos(2nt). \tag{4}$$

We suppose that all the motions of the ions except the micromotion (4) are frozen out (cold Coulomb crystal).

The main trap-induced corrections to the frequency $\nu=\omega/2\pi$ of the clock transition of the ith ion are the micromotion-induced second-order Doppler shift $\Delta\nu_{\rm D}^i$, and the Stark shift $\Delta\nu_{\rm S}^i$ caused by the time-dependent local electric field of the trap and nearby ions acting on the ith ion at its instantaneous position. The second-order fractional Doppler shift averaged over the period of the micromotion is

$$\frac{\Delta\nu_{\rm D}^i}{\nu}=-\frac{\Omega^2\ell^2}{4}\frac{\langle\dot{\bar{r}}^2\rangle}{2c^2}=-\frac{\Omega^2\ell^2}{c^2}\sum_{n=1}^{\infty}n^2\bar{R}_{2n,i}^2, \tag{5}$$

where c is the speed of light, and the prefactor comes from the scaling (2).

We first consider the Stark shift of the clock transition caused by the local electric field acting on the ion. Following Ref. [26], we suppose that the ion trap is placed into a homogeneous external magnetic field $\bar{B}$ causing the Zeeman splitting to be much larger than the tensor component of the Stark shift (see estimations at the end of Sec. V). Then the Stark shift of some Zeeman sublevel can be written as

$$\Delta\mathcal{E}=-\frac{\alpha_0}{2}\bar{E}^2-\frac{\alpha_2}{4}\left(3E_z^2-\bar{E}^2\right), \tag{6}$$

where the axis z is oriented along $\bar{B}$, α_0 is the scalar polarizability, and α_2 is

$$\begin{aligned}\alpha_2&=\alpha_2(\eta,J,F,m_F)\\&=\alpha_{\rm tens}(\eta,J)\frac{3m_F^2-F(F+1)}{3F^2-F(F+1)}(-1)^{I+J+F}\begin{Bmatrix}F & J & I\\ J & F & 2\end{Bmatrix}\\&\quad\times\left(\frac{F(2F-1)(2F+1)(2J+3)(2J+1)(J+1)}{(2F+3)(F+1)J(2J-1)}\right)^{1/2}.\end{aligned} \tag{7}$$

Here η, J, F, and m_F are the principal quantum number, the angular momentum of the electronic shell, the total angular momentum, and its projection onto the direction of the magnetic field, respectively, and $\alpha_{\rm tens}(\eta,J)$ is the tensor polarizability characterizing the state η,J of the electronic shell of the atom [26].

Denoting the differential polarizabilities $\Delta\alpha_k=\alpha_k^u-\alpha_k^l$ ($k=0$ or 2) of the upper (u) and lower (l) clock states, and taking into account the relation between the local electric field and the instantaneous acceleration of the ion, we can write the time-averaged scalar and tensor Stark shifts, $\Delta\nu_{\rm S,0}^i$ and $\Delta\nu_{\rm S,2}^i$, of the clock transition of the ith ion as

$$\begin{aligned}\Delta\nu_{\rm S,0}^i&=-\frac{\Delta\alpha_0}{4\pi\hbar}\langle\bar{E}^2\rangle=-\frac{\Delta\alpha_0}{4\pi\hbar}\frac{\Omega^4\ell^2m^2}{16q^2}\langle\ddot{\bar{r}}^2\rangle\\&=-\frac{\Delta\alpha_0}{2\pi\hbar}\frac{\Omega^4\ell^2m^2}{q^2}\sum_{n=1}^{\infty}n^4\bar{R}_{2n,i}^2,\end{aligned} \tag{8}$$

$$\Delta\nu^i_{S,2} = \frac{\Delta\alpha_2}{8\pi\hbar}\left(\langle\bar{E}^2\rangle - 3\langle\bar{E}_z^2\rangle\right) = \frac{\Delta\alpha_2}{4\pi\hbar}\frac{\Omega^4\ell^2m^2}{q^2}\sum_{n=1}^{\infty}n^4\left(\bar{R}^2_{2n,i} - 3Z^2_{2n,i}\right), \quad (9)$$

where $Z_{2n,i}$ is the z projection of $R_{2n,i}$.

Combining Eqs. (5), (8), and (9), we can express the sum of the Doppler and Stark shifts in the form

$$\Delta\nu^i = \Delta\nu^i_S + \Delta\nu^i_D = -\frac{\Omega^2\ell^2\nu}{c^2}\left[1 + \left(\Delta\alpha_0 - \frac{\Delta\alpha_2}{2}\right)\frac{(m\Omega c)^2}{2\pi\hbar\nu q^2}\right]\sum_{n=1}^{\infty}n^4\bar{R}^2_{2n,i} + \frac{\Omega^2\ell^2\nu}{c^2}\sum_{n=1}^{\infty}(n^4-n^2)\bar{R}^2_{2n,i} - 3\Delta\alpha_2\frac{\Omega^4m^2\ell^2}{4\pi\hbar q^2}\sum_{n=1}^{\infty}Z^2_{2n,i}n^4. \quad (10)$$

It is easy to see that if $\Delta\alpha_2 > 2\Delta\alpha_0$, the first term in Eq. (10) will be zero at the so-called magic value Ω_0 of the radio frequency Ω:

$$\Omega_0 = \frac{q}{mc}\sqrt{\frac{4\pi\hbar\nu}{\Delta\alpha_2 - 2\Delta\alpha_0}}. \quad (11)$$

In the next section we consider remaining terms of Eq. (10).

III. RESIDUAL MICROMOTION-RELATED SHIFTS

To estimate residual terms in Eq. (10), we expand $\bar{R}^2_{2n,i}$ and $Z^2_{2n,i}$ by the small parameter $\epsilon = 2\omega_z/\Omega$. Also we suppose that the amplitudes $\bar{R}_{2n,i}$ $(n \neq 0)$ of the oscillating terms are small in comparison with the time-independent components $R_{0,i}$. Then we can decompose the right part of EOM (3) as

$$\frac{\bar{r}_{ij}}{r^3_{ij}} = \frac{\bar{R}_{0,ij}}{R^3_{0,ij}} + \bar{\bar{Q}}_{ij}\cdot\bar{r}'_{ij} + \cdots, \quad (12)$$

where $\bar{r}'_{ij} = \bar{r}_{ij} - \bar{R}_{0,ij}$, and

$$\bar{\bar{Q}}_{ij} = -\frac{3\bar{R}_{0,ij}\otimes\bar{R}_{0,ij} - \bar{\bar{I}}R^2_{0,ij}}{R^5_{0,ij}}. \quad (13)$$

Here the symbol $\otimes$ denotes the outer product, and $\bar{\bar{I}}$ is the identity matrix.

Substituting Eqs. (13) and (4) into Eq. (3), we obtain

$$\bar{R}_{2,i} = \frac{\epsilon}{4}\bar{\bar{\Lambda}}_{rf}\cdot\bar{R}_{0,i} + \frac{\epsilon^3}{16}\left[\left(\bar{\bar{\Lambda}}_s + \frac{\bar{\bar{\Lambda}}^2_{rf}}{16}\right)\cdot\bar{\bar{\Lambda}}_{rf}\cdot\bar{R}_{0,i} - \sum_{j\neq i}\bar{\bar{Q}}_{ij}\cdot\bar{\bar{\Lambda}}_{rf}\cdot\bar{R}_{0,ij}\right] + O(\epsilon^5), \quad (14)$$

$$\bar{R}_{4,i} = \frac{\epsilon^2}{64}\bar{\bar{\Lambda}}^2_{rf}\cdot\bar{R}_{0,i} + O(\epsilon^4), \quad (15)$$

$$\bar{R}_{6,i} = \frac{\epsilon^3}{2304}\bar{\bar{\Lambda}}^3_{rf}\cdot\bar{R}_{0,i} + O(\epsilon^5). \quad (16)$$

Consider the two residual terms in Eq. (10). The second term contains only the summands with $n \geqslant 2$. It may be estimated as

$$\frac{\nu\Omega^2\ell^2}{c^2}\sum_{n=1}^{\infty}(n^4-n^2)\bar{R}^2_{2n,i} \approx 12\frac{\nu\Omega^2\ell^2}{c^2}\bar{R}^2_{4,i} \approx \frac{3\nu\epsilon^4}{1024}\frac{\Omega^2\ell^2}{c^2}\bar{R}_{0,i}\cdot\bar{\bar{\Lambda}}^4_{rf}\cdot\bar{R}_{0,i}. \quad (17)$$

The last term of Eq. (10),

$$-3\Delta\alpha_2\frac{\Omega^4m^2\ell^2}{4\pi\hbar q^2}\sum_{n=1}^{\infty}Z^2_{2n,i}n^4, \quad (18)$$

contains also the summand with $n = 1$, which is proportional to ϵ^2. However, it can be substantially reduced by a proper choice of the trap geometry. Namely, if the radio-frequency component of the trap field is orthogonal to the z axis (see Fig. 1), i.e., if

$$\bar{\bar{\Lambda}}_{rf} = \begin{bmatrix} a & 0 & 0\\ 0 & -a & 0\\ 0 & 0 & 0\end{bmatrix}, \quad (19)$$

then $Z_{6,i} = O(\epsilon^4)$, $Z_{4,i} = O(\epsilon^4)$, and $Z_{2,i} = O(\epsilon^3)$. Therefore, the whole last term of Eq. (10) is of the order of ϵ^6, and it is dominated by the second term of Eq. (10). We can neglect it, and approximate $\Delta\nu^i$ as

$$\Delta\nu^i \approx \frac{3\nu\epsilon^4}{1024}\frac{\Omega^2\ell^2}{c^2}a^4\left(X^2_{0,i} + Y^2_{0,i}\right). \quad (20)$$

For our future estimations we consider the particular case of a spherical trap. Namely, we take $a = \sqrt{3}$ in Eq. (19), and

$$\bar{\bar{\Lambda}}_s = \begin{bmatrix} -\frac{1}{2} & 0 & 0\\ 0 & -\frac{1}{2} & 0\\ 0 & 0 & 1\end{bmatrix}, \quad (21)$$

which corresponds to the pseudopotential

$$V(\bar{r}) = \frac{m\omega_z^2}{2}\bar{r}\cdot\left(\bar{\bar{\Lambda}}_s + \frac{\bar{\bar{\Lambda}}^2_{rf}}{2}\right)\cdot\bar{r} = \frac{m\omega_z^2\bar{r}^2}{2}. \quad (22)$$

It is easy to show that a large Coulomb crystal of N ions in such a trap will have an approximate spherical shape with the radius

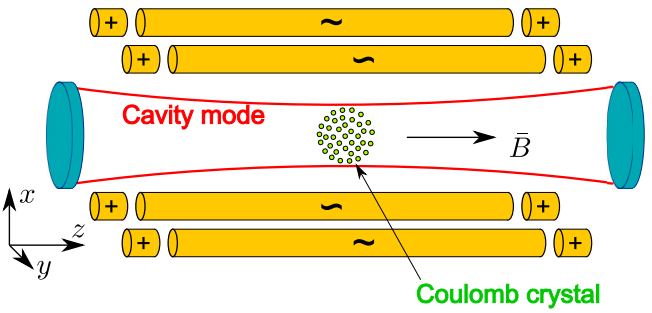

FIG. 1. Sketch of the linear Paul trap with Coulomb crystal and external cavity (not to scale), where the $|F_u, m_u = 0\rangle \rightarrow |F_l, m_l = \pm 1\rangle$ quadrupole transitions are coupled with two circularly polarized cavity modes. $\bar{B}$ is the magnetic field determining the quantization axis.

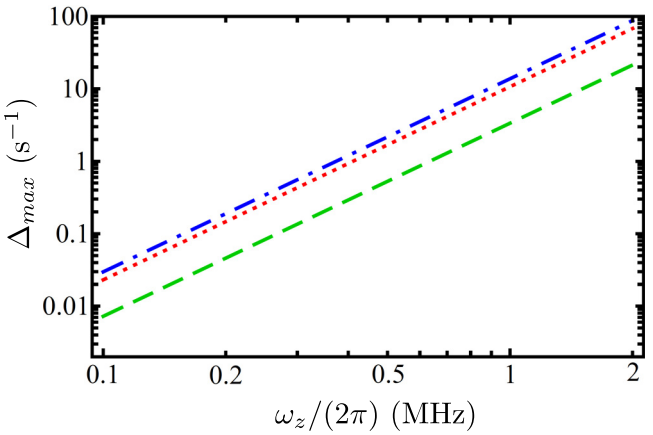

FIG. 2. Maximum micromotion-induced shift $\Delta_{\max}$ calculated according to Eq. (23) at $N = 1 \times 10^5$ ions for different $|^3D_2, F_u, m_F = 0\rangle \rightarrow |^1S_0, F_l = 7, m_F = 1\rangle$ transitions in $^{176}Lu^+$ ions. Red dotted line, $F_u = 5$, $\Omega = 2\pi \times 25.3$ MHz; green dashed line, $F_u = 8$, $\Omega = 2\pi \times 55.3$ MHz; blue dot-dashed line, $F_u = 9$, $\Omega = 2\pi \times 22.3$ MHz.

$R \approx N^{1/3}$ in units of ℓ (i.e., ℓ is the Wigner-Seitz radius), and the density of the crystal will be homogeneous on the scales exceeding ℓ.

The micromotion-related shift (20) goes to zero at the center of the crystal and reaches its maximum value

$$\Delta_{\max} = 2\pi\, \Delta\nu^i_{\max} \approx \left(\frac{3}{4}\right)^3 \frac{2\pi\, v\, N^{2/3}\, \omega_z^{8/3}\, q^{4/3}}{\Omega_0^2\, c^2\, m^{2/3}} \tag{23}$$

at $X_{0,i}^2 + Y_{0,i}^2 = N^{2/3}$.

To illustrate the dependence of $\Delta_{\max}$ on ω_z, we present in Fig. 2 the maximal micromotion-related shifts $\Delta_{\max}(\omega_z)$ for different $|^3D_2, F_u, m_F = 0\rangle \rightarrow |^1S_0, F_l, m_F = 1\rangle$ transitions in $^{176}Lu^+$ ions, supposing that the spherical Coulomb crystal contains $N = 1 \times 10^5$ ions, and that the radio frequencies Ω are equal to the magic frequencies Ω_0 for the corresponding transitions; see Sec. V for details.

We should note that expressions (20)–(23) for the micromotion-related shift as well as for the magic frequency Ω_0 [Eq. (11)] of the radio-frequency field have been obtained in the leading order (ϵ^4) of the small parameter ϵ, and in this leading order the individual shift $\Delta_i \propto X_i^2 + Y_i^2$. However, it is easy to see that the first term in Eq. (10) (which turns to zero at $\Omega = \Omega_0$) is also proportional to $X^2 + Y^2$ in the leading order of ϵ^2. Therefore, fine tuning of Ω near Ω_0 may be used for further compensation of the micromotion-related shifts down to the order of ϵ^6; the respective correction of the magic frequency was considered in Ref. [23]. Also, this tuning may be used for compensation of the light shifts caused by the pumping and cooling fields, or for suppression of the sensitivity of the frequency of the lasing transition to fluctuations of nonperfectly controlled parameters of the trap, such as amplitudes of the trapping and pumping fields. Detailed investigations of these possibilities are beyond the scope of this paper.

IV. CAVITY FIELD

In this section we estimate the output power of the bad-cavity laser based on a spherical Coulomb crystal with radius $R_c = N^{1/3}\ell$ coupled with the cavity field. We neglect here the micromotion-induced and quadrupole shifts of the lasing transitions; this assumption is acceptable, if the inhomogeneous broadening caused by these shifts is small in comparison with the homogeneous one [24]. These assumptions are proved in the end of Sec. V. Instead, we take into account that the cavity mode is a standing-wave Gaussian mode with waist w_0.

We start from the mean-field equations (see Appendix A for details of the derivation), where we neglect detunings and suppose equivalence of the cavity eigenfrequency ω_c with the transition frequencies ω and ω_{ul}^j of the laser field and lasing transitions:

$$\frac{d\langle\hat{c}\rangle}{dt} = -\frac{\kappa}{2}\langle\hat{c}\rangle - \frac{i}{2}\sum_j g_j\langle\hat{\sigma}_{lu}^j\rangle, \tag{24}$$

$$\frac{d\langle\hat{\sigma}_z^j\rangle}{dt} = ig_j\left[\langle\hat{c}^+\rangle\langle\hat{\sigma}_{lu}^j\rangle - \langle\hat{c}\rangle\langle\hat{\sigma}_{ul}^j\rangle\right] - \gamma_\parallel\langle\hat{\sigma}_z^j\rangle + w - \gamma, \tag{25}$$

$$\frac{d\langle\hat{\sigma}_{lu}^j\rangle}{dt} = \frac{ig_j}{2}\langle\hat{c}\rangle\langle\hat{\sigma}_z^j\rangle - \gamma_\perp\langle\hat{\sigma}_{lu}^j\rangle. \tag{26}$$

Here $\hat{c}$ and $\hat{c}^+$ are the cavity field operators, $\hat{\sigma}_{\alpha\beta}^j = |\alpha^j\rangle\langle\beta^j|$ ($|\alpha^j\rangle$ and $|\beta^j\rangle$ are the generic notations for the levels of the jth atom), $\langle\hat{\sigma}_z^j\rangle = \langle\hat{\sigma}_{uu}^j\rangle - \langle\hat{\sigma}_{ll}^j\rangle$, w is the incoherent pumping rate, γ is the spontaneous rate of the lasing transition, $\gamma_\parallel = w + \gamma$, $\gamma_\perp = (\gamma + w)/2 + \gamma_R$, γ_R is the incoherent dephasing rate (limited from the bottom by the value $\xi w/2$, where $\xi = \Gamma_1/\Gamma_2$ is the ratio of decay rates Γ_1 and Γ_2 of the intermediate pumping state into the lower and the upper lasing states $|l\rangle$ and $|u\rangle$, respectively), and g_j is the coupling coefficient of the cavity field with the lasing transition in the jth ion. As is shown in Appendix B,

$$g_j = g(\bar{r}) = g_0\, e^{-\frac{r_\perp^2}{w_0^2}} \cos(\bar{k}\cdot\bar{r}). \tag{27}$$

One may obtain the steady-state (cw) solution of Eqs. (24)–(26) setting time derivatives to zero. Then, from Eq. (24) follows

$$\langle\hat{c}\rangle_{\rm cw} = -\frac{i}{\kappa}\frac{3N}{4\pi R_c^3}\int_{-R_c}^{R_c}\int_0^{\sqrt{R_c^2-z^2}} g_j(\bar{r})\langle\hat{\sigma}_{lu}(g_j(\bar{r}))\rangle_{\rm cw} \times 2\pi\, r_\perp\, dr_\perp\, dz, \tag{28}$$

where $R_c = N^{1/3}\ell$ is the radius of the Coulomb crystal. In turn, $\langle\hat{\sigma}_{lu}(g_j(r))\rangle_{\rm cw} = \langle\hat{\sigma}_{lu}^j\rangle_{\rm cw}$ may be expressed via $\langle\hat{c}\rangle_{\rm cw}$ with the help of Eqs. (25) and (26) as

$$\langle\hat{\sigma}_{lu}(g_j(\bar{r}))\rangle_{\rm cw} = \frac{1}{2}\frac{ig_j(\bar{r})\langle\hat{c}\rangle_{\rm cw}(w-\gamma)}{\gamma_\perp\gamma_\parallel + |\langle\hat{c}\rangle_{\rm cw}|^2 g_j^2}. \tag{29}$$

Substituting Eq. (27) into Eq. (29) and Eq. (29) into Eq. (28) and reducing $\langle\hat{c}\rangle_{\rm cw}$, we obtain the equation

$$1 = \frac{(w-\gamma)}{2\kappa}\frac{3N}{4\pi R_c^3}\int_{-R_c}^{R_c}\int_0^{\sqrt{R_c^2-z^2}} 2\pi\, r_\perp \times \frac{g_0^2\cos^2(kz)e^{-\frac{2r_\perp^2}{w_0^2}}}{\gamma_\perp\gamma_\parallel + |\langle\hat{c}\rangle_{\rm cw}|^2 g_0^2\cos^2(kz)e^{-\frac{2r_\perp^2}{w_0^2}}}\, dr_\perp dz. \quad (30)$$

The integral over $r_\perp$ may be taken analytically. Then Eq. (30) transforms into

$$1 = \frac{(w-\gamma)}{2\kappa}\frac{3N}{4R_c^3}\frac{w_0^2}{2|\langle\hat{c}\rangle_{\rm cw}|^2} \times \int_{-R_c}^{R_c}\ln\left[\frac{\gamma_\perp\gamma_\parallel + |\langle\hat{c}\rangle_{\rm cw}|^2 g_0^2\cos^2(kz)}{\gamma_\perp\gamma_\parallel + |\langle\hat{c}\rangle_{\rm cw}|^2 g_0^2\cos^2(kz)e^{-2\frac{R_c^2-z^2}{w_0^2}}}\right]dz. \quad (31)$$

Because the cavity waist w_0 and the radius of the crystal, R_c, are large in comparison with $1/k$, we can average Eq. (31) on the scale of $2\pi/k$ with the help of the following relation:

$$\frac{2}{\pi}\int_0^{\pi/2}\ln(1+b\cos^2 z)dz = 2\ln\left[\frac{\sqrt{1+b}+1}{2}\right]. \quad (32)$$

It allows one to represent Eq. (31) in the form

$$1 = \frac{3N\zeta^2(w-\gamma)}{4\kappa|\langle\hat{c}\rangle_{\rm cw}|^2}[\ln(1+\sqrt{1+A}) - F(A,\zeta)], \quad (33)$$

where

$$F(A,\zeta) = \int_0^1 \ln\left(1+\sqrt{1+A\exp\frac{2(x^2-1)}{\zeta^2}}\right)dx, \quad (34)$$

$$A = \frac{|\langle\hat{c}\rangle_{cw}|^2 g_0^2}{\gamma_\parallel\gamma_\perp}, \quad (35)$$

$$\zeta = \frac{w_0}{R_c}. \quad (36)$$

To find the steady-state intracavity field, one has to solve Eq. (33) numerically.

V. PROSPECT FOR BAD-CAVITY LASER WITH $^{176}Lu^+$ IONS

In this section we consider the implementation of a bad-cavity laser using the $^3D_2 \to {}^1S_0$ transition in the $^{176}Lu^+$ ($I = 7$) ion. Briefly this possibility was mentioned in Ref. [24]; here we present a more detailed quantitative analysis.

A possible pumping scheme is shown in Fig. 3: A 350.84-nm pumping laser populates the $^3P_1^o$ state which decays with a 42% probability into the $^3D_2$ upper lasing state, and with a 37.6 % probability back into the lower lasing state [27]. The decay of the $^3P_1^o$ state will populate also the long-living $^3D_1$ state, which can be depopulated via the $^3P_2^o$ state with the help of a 484.10-nm laser. Two additional 661.37- and 547.82-nm lasers should be applied to pump the atoms out of the $^1D_2$ and $^3D_3$ states populated by the decay of the $^3P_2^o$ state. The 484.10-, 547.82-, and 661.37-nm lasers may be detuned to the red side and be used also for cooling of the ion ensemble; sympathetic cooling with an additional ion species is also possible.

An important point is that all involved states except the ground state have a hyperfine structure; therefore, the pumping lasers should have several frequency components to effectively repump the atoms. Finally, a five-component 499.55-nm laser should be employed to pump the populations into the upper lasing state, for example, with specific $F = F_u$ and $m_F = 0$. This can be realized if one component of this laser is tuned in resonance with the $|^3D_2, F_e\rangle \to |^3P_2^o, F_e\rangle$ transition and polarized along the z axis of the trap, coinciding with the direction of the auxiliary magnetic field.

For our calculations, we use values from Ref. [27], where the spontaneous rate of the $^3D_2 \to {}^1S_0$ lasing transition is $\gamma = 4.19\times10^{-2}$ s^{-1}, the differential scalar polarizability is $\Delta\alpha_0 = -0.9a_0^3$, and the tensor polarizability of the upper state is $\alpha_{\rm tens}(^3D_2) = -5.6a_0^3$, where a_0 is the Bohr radius.

Let the lower indices l and u correspond to the lower lasing $^1S_0$ and the upper lasing $^3D_2$ levels. With the help of the

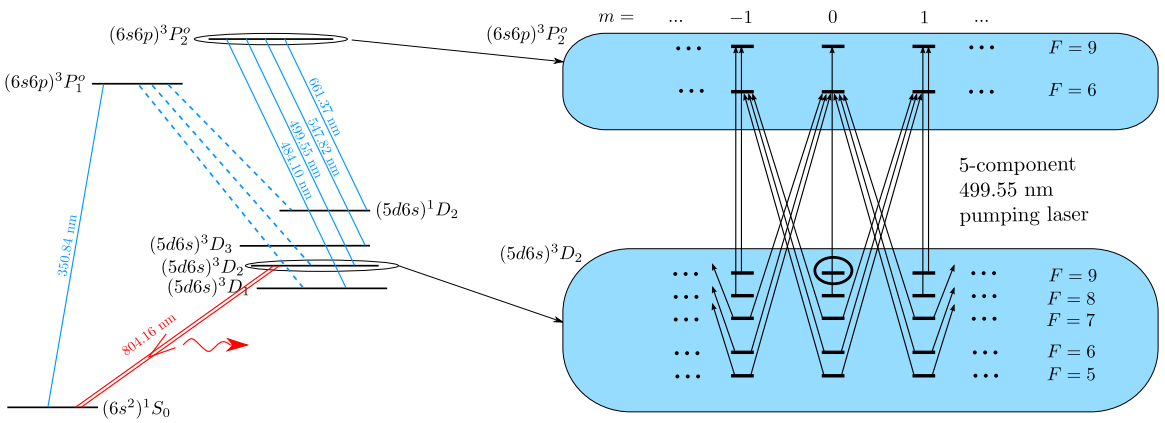

FIG. 3. Left: General pumping scheme (hyperfine structure not shown) for an 804-nm bad-cavity laser on ^{176}Lu ions. Dashed lines denote the most relevant spontaneous decays, and solid lines correspond to both spontaneous and laser-induced transitions (wavelengths are indicated). Right: Details of the hyperfine and Zeeman structure of $^3D_2$ and $^3P_2^o$ levels, and transitions induced by a five-component 499.55-nm pumping laser to pump the ions into the $|F_u = 9, m_u = 0\rangle$ upper lasing state.

499.55-nm laser, the populations may be pumped either into one of the $|^3D_2, F_u, m_F = \pm F_u\rangle$ states (both $m_F = \pm F_u$ states may also be populated simultaneously, if $F_u > 5$), or into some of the $|^3D_2, F_u, m_F = 0\rangle$ states.

Quadrupole transitions may, generally speaking, be accompanied by $\Delta m = 0, \pm 1, \pm 2$. In this paper we restrict our consideration to the geometry shown in Fig. 1. In such a configuration, micromotion of the ions takes place primarily in the plane orthogonal to the cavity axis [up to the terms of order ϵ^3; see Eqs. (14) and (15)], and the ions will be confined to length scales significantly smaller than the mode wavelength in the axial direction, i.e., in the Lamb-Dicke regime. As shown in Appendix B, only the transitions with $\Delta m = \pm 1$ will be coupled with the cavity modes in such a configuration.

Note that two modes (σ^+ and σ^- polarized) with the same eigenfrequency may be excited simultaneously in the cavity. These modes couple the upper $|^3D_2, F_u, m_F = 0\rangle$ lasing state with two $|^1S_0, F_l, m_l = \pm 1\rangle$ lower states, forming a "Λ system." Generally speaking, lasing in such a system cannot be represented as a simple superposition of two independent lasers, because the modes will be coupled via the coherence between two lower lasing levels. However, a detailed investigation of such a system lies beyond the scope of the present paper, and we consider only a single circularly polarized mode coupling $|u\rangle = |^3D_2, F_u, m_F = 0\rangle$ and $|l\rangle = |^1S_0, F_l = I, m_F = 1\rangle$ states. Note also that a selective excitation of a single mode may be performed if the mirrors of the optical cavity will have slightly different transparencies for left- and right-polarized modes, and the lasing threshold will be more easily attainable for one of them.

Using the method presented in Sec. II, we find that the magic frequency Ω_0 exists for $F_u = 5$, 8, and 9 ($\Omega_0 = 2\pi \times 25.3$, $\Omega_0 = 2\pi \times 45.3$, and $\Omega_0 = 2\pi \times 22.3$ MHz, respectively). Also, one may find the values of the "magic magnetic field" B_m, at which the sensitivity of the lasing transition frequency to the fluctuation of this field vanishes in the first order: $B_m = 0.388$, -1.035, and -1.040 G for $F_u = 5$, 8, and 9, respectively.

The maximal value g_0 of the coupling coefficient of the Gaussian standing-wave cavity mode with the lasing transition

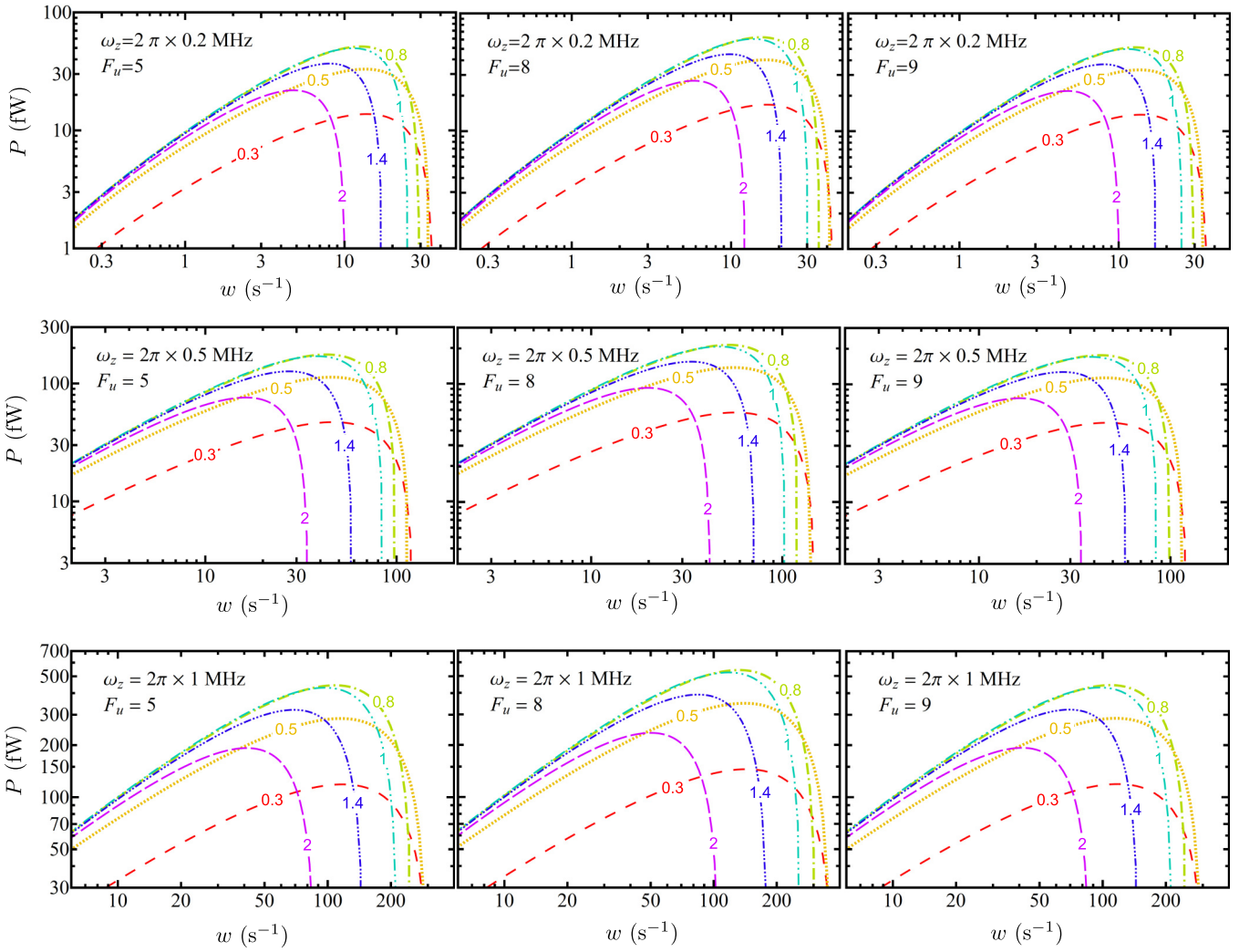

FIG. 4. Output power P for various confinement frequencies ω_z and upper lasing states $|F_u, m_F = 0\rangle$ (on different panels, see labels in upper left corners) and different values of $\zeta = w_0/R_c$ (different curves on the same plot, labeled by the values of ζ) as functions of the pumping rate w (x axis) for a spherical Coulomb crystal containing $N = 1 \times 10^5$ $^{176}Lu^+$ ions coupled to the cavity with finesse $\mathcal{F} = 1 \times 10^5$. Confinement frequencies are $\omega_z = 2\pi \times 0.2$, $\omega_z = 2\pi \times 0.5$, and $\omega_z = 2\pi \times 1$ MHz, which correspond to the radii $R_c = N^{1/3}\ell$ of the crystal equal to 368, 200, and 126 μm, respectively.

may be estimated as (see Appendix B for details)

$$g_0 = \Theta_{ul}\sqrt{\frac{5\pi c^3\gamma}{\omega^2 V_{\rm eff}}}, \tag{37}$$

where $V_{\rm eff} = \pi w_0^2 L$ is the effective mode volume, L is the cavity length, w_0 is the mode waist,

$$\Theta_{ul}^2 = 8(2F_l+1)(2J_u+1)\begin{Bmatrix} J_l & I & F_l \\ F_u & 2 & J_u \end{Bmatrix}^2 \times \left(C^{F_u m_u}_{F_l m_l 2 -1}\right)^2, \tag{38}$$

and $m_u = m_l - 1$. It is easy to see that the ratio g_0^2/κ does not depend on the cavity length L, but only on the cavity finesse $\mathcal{F}$, because κ may be expressed via L and $\mathcal{F}$ as $\kappa = \pi c/(\mathcal{F}L)$.

To study the dependence of the output power on the mode waist w_0, it is convenient to express w_0 via the radius R_c of the Coulomb crystal as $w_0 = \zeta R_c$, like in Sec. IV. The output power P may be estimated as

$$P = \hbar\omega\kappa\,|\langle\hat{c}\rangle_{\rm cw}|^2, \tag{39}$$

where $\langle\hat{c}\rangle_{\rm cw}$ is the steady-state intracavity field which may be found from the numeric solution of Eq. (33). Note also that $\langle\hat{c}\rangle_{\rm cw}$ appears in Eqs. (33)–(36) and (39) either as $|\langle\hat{c}\rangle_{\rm cw}|^2 g^2$ or as $|\langle\hat{c}\rangle_{\rm cw}|^2\kappa$; therefore, the output power depends on the cavity finesse $\mathcal{F}$, not on the length L.

For a quantitative estimation of the output power, we consider a spherical Coulomb crystal containing $N = 1\times 10^5$ ^{176}Lu$^+$ ions, where the lasing transition is one of the $|^3D_2, F_u, m_F = 0\rangle \to \rangle |^1S_0, F_l = I, m_F = 1\rangle$ quadrupole transitions with $F_u = 5$, 8, or 9. The cavity finesse is $\mathcal{F} = 1\times 10^5$. Also we suppose the repumping efficiency $\xi = 0.6$ (i.e., 40% of the atoms pumped into the $^3P_1^o$ state from the lower lasing state decay back; see Appendix A for details).

Figure 4 presents the output power P [Eq. (39)] for these three transitions for three different values of the confinement frequency ω_z ($\omega_z = 2\pi\times 200$ kHz, $\omega_z = 2\pi\times 500$ KHz, and $\omega_z = 2\pi\times 1$ MHz), and different values of ζ.

In Fig. 5 we show the dependence of the maximum output power $P_{\rm max}$, corresponding to the optimized pumping rate w, on the parameter ζ. One can see that the optimal values of ζ are about 0.8.

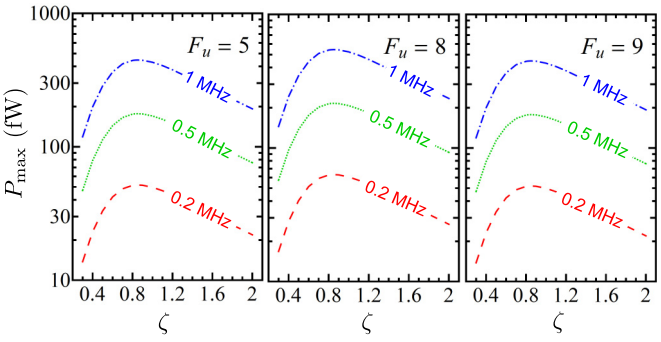

FIG. 5. Output power $P_{\rm max}$ optimized with respect to the pumping rate w as a function of $\zeta = w_0/R_c$ for different upper lasing states $|F_u, m_F = 0\rangle$ (on different panels; see labels in upper right corners) and different confinement frequencies ω_z (labeled curves on the same plot). Parameters are the same as in Fig. 4.

Let us discuss the linewidth $\Delta\omega$ of such a bad-cavity laser. Our semiclassical mean-field model cannot predict the linewidth; one needs to construct at least some "second-order theory" keeping second-order cumulants of the operators related to different ions, as it was done in Refs. [10,28], but with a larger amount of groups of ions with different coupling strengths (and shifts, generally speaking). Such a task claims additional attention. However, as an order-of-magnitude estimation, we can take the formula

$$\Delta\omega \approx g^2/\kappa \tag{40}$$

from Ref. [10] and substitute g_0 for g. For $w_0 = 100$ μm (which corresponds to $\zeta = 0.8$ for a spherical Coulomb crystal with $N = 1\times 10^5$ ions at $\omega_z = 2\pi\times 1$ MHz) this estimation gives $\Delta\omega \sim 2\pi\times 3$ to $2\pi\times 4$ mHz for the transitions considered in this section; weaker confinement results in an even narrower linewidth.

Concerning the validity of negligence of the micromotion-induced frequency shift, the optimal values of the repumping rate w, at which the maximum output powers are attained, are about 15, 50, and 150 s^{-1} for $\omega_z = 2\pi\times 0.2$, $2\pi\times 0.5$, and $2\pi\times 1$ MHz, respectively. These values of w significantly exceed the maximum micromotion-induced shifts $\Delta_{\rm max}$ corresponding to the respective confinement frequencies; see Fig. 2. The repumping rate determines the homogeneous broadening; therefore, near the optimal regime we may neglect the inhomogeneous broadening related to the micromotion-induced shifts, at least for the parameters considered above.

A few words about the quadrupole shift are in order. This shift was investigated in Ref. [23] for the $^1S_0 \to {}^3D_1$ transition in the Lu$^+$ ion. It has been shown that, for $\omega_z = 2\pi\times 200$ kHz and a spherical Coulomb crystal with more than a thousand ions, the distribution of the quadrupole shift is symmetric and has a dispersion below 0.1 Hz. The quadrupole shift scales as ℓ^{-3}, or as ω_z^2. Because the quadrupole moment of the $^3D_1$ and $^3D_2$ states are similar, we estimate that for $\omega_z = 2\pi\times 1$ MHz the dispersion of the quadrupole shifts does not exceed a few hertz, which is much less than the optimal repumping rate.

Finally, let us compare the Zeeman splitting with the tensor Stark shift. One can easily calculate the Zeeman shifts between the upper lasing state $|F_u, m_F = 0\rangle$ and the nearby Zeeman state $|F_u, m_F = 1\rangle$ at the respective "magic" value of the magnetic field B_z: they are 211, 258, and 377 kHz, respectively. At the same time, at $\omega_z = 2\pi\times 1$ MHz and $N = 1\times 10^5$, the tensor Stark shift will be only about 1 kHz on the edge of the Coulomb crystal. Therefore, the tensor Stark shift is small in comparison with the Zeeman shift, and the theory in Ref. [26] may be applied.

VI. DISCUSSION AND CONCLUSION

In the present paper, we studied the possibility to create a bad-cavity laser on forbidden transitions in cold ions trapped in a linear Paul trap and forming a large Coulomb crystal. We considered the particular case of a spherical Coulomb crystal of ^{176}Lu$^+$ ions, where the $|^3D_2, F_u, m_F = 0\rangle \to |^1S_2, F_l = I, m_F = 1\rangle$ transition is coupled to the circularly polarized mode of the high-finesse ($\mathcal{F} = 1\times 10^5$) optical cavity, whose axis coincides with the trap axis and with the direction of external magnetic field. We showed that 1×10^5 ions in the

trap with $\omega_z = 2\pi \times 1$ MHz may provide about 0.5 pW of output power with a 150 s^{-1} repumping rate if the mode waist w_0 is about 80% of the crystal radius, i.e., $w_0 \sim 100\ \mu$m.

To increase this power, one could increase the number of ions, increase the frequency ω_z of the radial confinement, or use an elongated trap. Here we consider the main advantages and disadvantages of these measures in some detail.

First, the ion crystal radius R_c scales as $R_c \propto N^{1/3}$. To keep the value $\zeta = R_c/w_0$ near the optimum (about 0.8), we have to increase the cavity waist $w_0 \propto N^{1/3}$, so the coupling coefficient $g \propto N^{-1/3}$. The total output power $P \propto N^2 g^2$ [10], which gives the scaling law $P \propto N^{4/3}$. Also, in larger ion ensembles, the maximum micromotion-related shifts grow with N, particularly $\Delta_{\max} \propto N^{2/3}$ at $\Omega = \Omega_0$ [Eq. (23)]. At the same time, a decrease of g may lead to a decrease of the linewidth $\delta\omega$, as shown in Eq. (40). We should note, however, that both controlling a large number of ions and fabricating a high-finesse resonator with a large mode waist may be technically challenging.

Second, increasing the confinement frequency ω_z will lead to a scaling $R_c \propto \omega_z^{-2/3}$, which allows one to increase the coupling coefficient $g \propto \omega_z^{2/3}$, keeping the same ζ, so that the output power scales as $P \propto \omega_z^{4/3}$. At the same time, the maximal micromotion-induced shift $\Delta_{\max}$ at $\Omega = \Omega_0$ will scale as $\Delta_{\max} \propto \omega_z^{8/3}$, as shown in Eq. (23). Using the semiclassical model with equal coupling g for all the atoms, but with nonzero frequency shifts [Eq. (20)], we found that the maximum output power might be attained at $\omega_z \sim 2\pi \times 10$ to $2\pi \times 20$ MHz (for different transitions) if the other parameters are the same as considered in Sec. V. However, such a large value of ω_z is much higher than typical ion trap axial frequencies [23,25]. Moreover, the parameter ϵ is no longer a small parameter at such large ω_z, and the theory presented in Secs. II and III is not valid. Finally, the increasing g may lead to a drastic increase of the linewidth $\Delta\omega$.

Third, the Coulomb crystal in the elongated trap will be less regular than in the spherical one, and the quadrupole shifts may play a more significant, non-negligible role. On the other hand, such a method allows one to pack more ions into the same cavity mode. Such a setup should be designed carefully.

In the present paper, we neglect the excitation of the second circularly polarized mode in the cavity. If such a mode will be excited, it will lead to a reduction of the output power. The picture will become more complex because of interactions of these modes via the coherence between the lower lasing states. A detailed investigation of their interaction will be presented in future work. Here we can note that both the output fields will have different polarizations and frequencies, and the frequency difference will be of the order of a few hundred hertz (for "magic" magnetic fields). The beat signal between two modes may be used for a stabilization of the magnetic field near its magic value.

In addition to $^{176}Lu^+$, some other ions with metastable states and negative differential polarizabilities may also be considered candidates, although it seems to be less straightforward to find a proper repumping scheme. Instead, one may implement a "passive" scheme with cavity-enhanced nonlinear spectroscopy, similar to the one proposed in Refs. [29,30]. Such a scheme may also be used for locking the frequency of some slave laser to the optical transition, and this approach does not require pumping of the atoms into the upper lasing state.

We considered the "collinear" configuration, where the trap axis, cavity axis, and external magnetic field are coaligned. In such a configuration, the cavity mode will be coupled only with $\Delta m = \pm 1$ quadrupole transitions. To allow the coupling with $\Delta m = 0$ and/or $\Delta m = \pm 2$ transitions, some nonzero angle between the cavity axis and the magnetic field should be introduced. It may be attained, for example, by tilting the cavity axis with respect to magnetic field, coaligned with the trap axis, or by tilting the magnetic field with respect to the cavity axis coinciding with the trap axis.

In the first case (tilted cavity) the broadening related to the tensor Stark shift [the third term in Eq. (10)] will be suppressed, as well as in the collinear configuration considered in the main text. However, such a scheme does not allow the use of an elongated trap geometry and will cause additional problems connected with confinement of the atoms to the Lamb-Dicke regime along the cavity axis. In particular, our estimations show that for the parameters of the ions considered in the paper, the amplitude $R_{2,i}\ell$ of the micromotion on the edges of the crystal exceeds the wavelength of the mode. Note that this micromotion-related issue may be of less importance for some long-wavelength transitions, such as $^2D_{3/2} \rightarrow {}^2S_{1/2}$ and $^2D_{5/2} \rightarrow {}^2S_{1/2}$ transitions in Ba^+ ions.

Tilting the magnetic field instead of the cavity axis allows the use elongated traps and keeps the ions in the Lamb-Dicke regime but requires special measures to suppress the tensor Stark shift. As shown in Ref. [31], compensation of this shift may be performed with a special choice of the magnetic field.

In summary, we have shown that a bad-cavity laser may be realized on a Coulomb crystal composed of ions with negative differential polarizability of the clock transition. As an example, we considered the $^3D_2 \rightarrow {}^1S_0$ lasing transition in $^{176}Lu^+$, with the ions forming a spherical Coulomb crystal in a linear Paul trap. Such a crystal may provide a route to truly steady-state lasing in the bad-cavity regime if the proper continuous cooling and pumping is performed.

ACKNOWLEDGMENTS

We are grateful to Murray Douglas Barrett and John Bollinger for fruitful discussion and valuable comments, and to Athreya Shankar for useful remarks. The study has been supported by the EU–FET-Open Project No. 664732 NuClock.

APPENDIX A: SEMICLASSICAL EQUATIONS FOR THREE-LEVEL MODEL AND ADIABATIC ELIMINATION OF THE INTERMEDIATE STATE

Consider the system of N three-level trapped atoms (ions) with states $|l\rangle$, $|u\rangle$, and $|i\rangle$, whose $|u\rangle \rightarrow |l\rangle$ transition is coupled with the cavity mode $\hat{c}$, and whose $|l\rangle \rightarrow |i\rangle$ transition is pumped by external field with Rabi frequency V; see Fig. 6. Neglecting the dipole-dipole interaction between different atoms and their collective coupling to the bath modes (the role of these effects are considered in Refs. [32,33]), we can

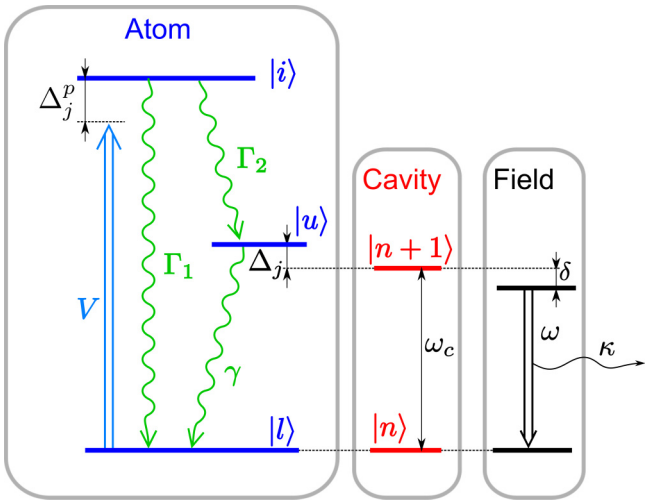

FIG. 6. Level structure and notations used for levels, frequencies, detunings, and relaxation rates: ω_c and ω are the frequencies of the cavity mode and the output laser field, Δ_j and Δ_j^p are the detunings of respective atomic transitions from the output and pumping fields, respectively, and Γ_1, Γ_2, and γ are the decay rates.

write the master equation for such a system in the form

$$\frac{d\rho}{dt} = -\frac{i}{\hbar}[\hat{\mathcal{H}},\hat{\varrho}] + \hat{\hat{\mathcal{L}}}_c[\hat{\varrho}] + \sum_j \hat{\hat{\mathcal{L}}}_j[\hat{\varrho}], \tag{A1}$$

where the Lindbladian $\hat{\hat{\mathcal{L}}}_c$ describes the relaxation of the cavity field,

$$\hat{\hat{\mathcal{L}}}_c[\hat{\varrho}] = -\frac{\kappa}{2}[\hat{c}^+\hat{c}\,\hat{\varrho} + \hat{\varrho}\,\hat{c}^+\hat{c} - 2\,\hat{c}\,\hat{\varrho}\,\hat{c}^+], \tag{A2}$$

the Lindbladian $\hat{\hat{\mathcal{L}}}_j$ describes the relaxations of individual atoms,

$$\begin{aligned}\hat{\hat{\mathcal{L}}}_j[\hat{\varrho}] = {}& \frac{\gamma}{2}\big[2\hat{\sigma}_{lu}^j\hat{\varrho}\hat{\sigma}_{ul}^j - \hat{\sigma}_{uu}^j\hat{\varrho} - \hat{\varrho}\hat{\sigma}_{uu}^j\big] \\ & + \frac{\Gamma_1}{2}\big[2\hat{\sigma}_{li}^j\hat{\varrho}\hat{\sigma}_{il}^j - \hat{\sigma}_{ii}^j\hat{\varrho} - \hat{\varrho}\hat{\sigma}_{ii}^j\big] \\ & + \frac{\Gamma_2}{2}\big[2\hat{\sigma}_{ui}^j\hat{\varrho}\hat{\sigma}_{iu}^j - \hat{\sigma}_{ii}^j\hat{\varrho} - \hat{\varrho}\hat{\sigma}_{ii}^j\big],\end{aligned} \tag{A3}$$

and the Hamiltonian in the respective rotating frame has the form

$$\begin{aligned}\hat{\mathcal{H}} = {}& \hbar\delta\hat{c}^+\hat{c} + \hbar\sum_j\big((\Delta_j+\delta)\hat{\sigma}_{uu}^j + \Delta_j^p\hat{\sigma}_{ii}^j\big) \\ & + \frac{\hbar}{2}\sum_j g_j\big(\hat{c}^+\hat{\sigma}_{lu}^j + \hat{\sigma}_{ul}^j\hat{c}\big) + \frac{\hbar V}{2}\sum_j\big(\hat{\sigma}_{il}^j + \hat{\sigma}_{li}^j\big).\end{aligned} \tag{A4}$$

Here and below we use the notation $\hat{\sigma}_{rq}^j = |r^j\rangle\langle q^j|$, where g_j is the coupling strength between the lth lower and uth upper lasing states and the cavity field, and V is the Rabi frequency of the pumping field.

In the semiclassical (mean-field) approximation, where all the correlators are decoupled, the set of equations for atomic and field expectation values is

$$\frac{d\langle\hat{c}\rangle}{dt} = -i\Big[\frac{\kappa}{2} + i\delta\Big]\langle\hat{c}\rangle - \frac{i}{2}\sum_j g_j\langle\hat{\sigma}_{lu}^j\rangle, \tag{A5}$$

$$\begin{aligned}\frac{d\langle\hat{\sigma}_{ll}^j\rangle}{dt} = {}& -i\frac{g_j}{2}\big[\langle\hat{c}^+\rangle\langle\hat{\sigma}_{lu}^j\rangle - \langle\hat{c}\rangle\langle\hat{\sigma}_{ul}^j\rangle\big] - \frac{iV}{2}\big[\langle\hat{\sigma}_{li}^j\rangle - \langle\hat{\sigma}_{il}^j\rangle\big] \\ & + \gamma\langle\hat{\sigma}_{uu}^j\rangle + \Gamma_1\langle\hat{\sigma}_{ii}^j\rangle,\end{aligned} \tag{A6}$$

$$\frac{d\langle\hat{\sigma}_{uu}^j\rangle}{dt} = i\frac{g}{2}\big[\langle\hat{c}^+\rangle\langle\hat{\sigma}_{lu}^j\rangle - \langle\hat{c}\rangle\langle\hat{\sigma}_{ul}^j\rangle\big] - \gamma\langle\hat{\sigma}_{uu}^j\rangle + \Gamma_2\langle\hat{\sigma}_{ii}^j\rangle, \tag{A7}$$

$$\frac{d\langle\hat{\sigma}_{ii}^j\rangle}{dt} = \frac{iV}{2}\big[\langle\hat{\sigma}_{li}^j\rangle - \langle\hat{\sigma}_{il}^j\rangle\big] - \Gamma\langle\hat{\sigma}_{ii}^j\rangle, \tag{A8}$$

$$\begin{aligned}\frac{d\langle\hat{\sigma}_{lu}^j\rangle}{dt} = {}& -\Big(\frac{\gamma}{2} + i(\Delta_j+\delta)\Big)\langle\hat{\sigma}_{lu}^j\rangle - \frac{ig_j}{2}\langle\hat{c}\rangle\big[\langle\hat{\sigma}_{ll}^j\rangle - \langle\hat{\sigma}_{uu}^j\rangle\big] \\ & + \frac{iV}{2}\langle\hat{\sigma}_{iu}^j\rangle,\end{aligned} \tag{A9}$$

$$\begin{aligned}\frac{d\langle\hat{\sigma}_{li}^j\rangle}{dt} = {}& -\Big(\frac{\Gamma}{2} + i\Delta_j^p\Big)\langle\hat{\sigma}_{li}^j\rangle + \frac{ig_j}{2}\langle\hat{c}\rangle\langle\hat{\sigma}_{ui}^j\rangle \\ & - \frac{iV}{2}\big[\langle\hat{\sigma}_{ll}^j\rangle - \langle\hat{\sigma}_{ii}^j\rangle\big],\end{aligned} \tag{A10}$$

$$\begin{aligned}\frac{d\langle\hat{\sigma}_{ui}^j\rangle}{dt} = {}& -\Big(\frac{\gamma+\Gamma}{2} + i\big(\Delta_j^p - \Delta_j - \delta\big)\Big)\langle\hat{\sigma}_{ui}^j\rangle \\ & + \frac{ig_j}{2}\langle\hat{c}\rangle\langle\hat{\sigma}_{li}^j\rangle - \frac{iV}{2}\langle\hat{\sigma}_{ul}^j\rangle,\end{aligned} \tag{A11}$$

plus respective equations for $\langle\hat{\sigma}_{ul}^j\rangle$, $\langle\hat{\sigma}_{il}^j\rangle$, and $\langle\hat{\sigma}_{iu}^j\rangle$. Here $\Gamma = \Gamma_1 + \Gamma_2$ is the total decay rate of the intermediate state $|i\rangle$.

Supposing that $\Gamma \gg (V,\Delta_j^p) \gg (g_j\langle\hat{c}\rangle,\Delta_j,\delta,\gamma)$, we can adiabatically eliminate the intermediate level $|i\rangle$ using Eqs. (A9)–(A11) and corresponding conjugated equations. It gives

$$\langle\hat{\sigma}_{li}^j\rangle = \langle\hat{\sigma}_{il}^j\rangle^* = \frac{-iV}{\Gamma + 2i\Delta_j^p}\langle\hat{\sigma}_{ll}^j\rangle, \tag{A12}$$

$$\langle\hat{\sigma}_{ii}^j\rangle = \frac{V^2}{\Gamma^2 + 4{\Delta_j^p}^2}\langle\hat{\sigma}_{ll}^j\rangle, \tag{A13}$$

$$\langle\hat{\sigma}_{ui}^j\rangle = \langle\hat{\sigma}_{iu}^j\rangle^* = \frac{-iV}{\Gamma + 2i\Delta_j^p}\langle\hat{\sigma}_{ul}^j\rangle. \tag{A14}$$

Substituting Eqs. (A12)–(A14) into Eqs. (A6)–(A8), we obtain

$$\begin{aligned}\frac{d\langle\hat{\sigma}_z^j\rangle}{dt} = {}& ig_j\big[\langle\hat{c}^+\rangle\langle\hat{\sigma}_{lu}^j\rangle - \langle\hat{c}\rangle\langle\hat{\sigma}_{ul}^j\rangle\big] \\ & + w\big[1 - \langle\hat{\sigma}_z^j\rangle\big] - \gamma\big[1 + \langle\hat{\sigma}_z^j\rangle\big],\end{aligned} \tag{A15}$$

$$\begin{aligned}\frac{d\langle\hat{\sigma}_{lu}^j\rangle}{dt} = {}& \frac{ig_j}{2}\langle\hat{c}\rangle\langle\hat{\sigma}_z^j\rangle \\ & - \Big(\frac{\gamma+w}{2} + \gamma_R + i\big(\Delta_j + \delta + \Delta_j^{\mathrm{LS}}\big)\Big)\langle\hat{\sigma}_{lu}^j\rangle.\end{aligned} \tag{A16}$$

Here $\langle\hat{\sigma}_z^j\rangle = \langle\hat{\sigma}_{uu}^j\rangle - \langle\hat{\sigma}_{ll}^j\rangle$,

$$w = \frac{\Gamma_2 V^2}{\Gamma^2 + 4\Delta_j^{p2}} \quad \text{and} \quad \Delta_j^{\mathrm{LS}} = \frac{w(\xi+1)}{\Gamma}\Delta_j^p \tag{A17}$$

are the incoherent pumping rate and the light shift,

$$\gamma_R = \xi w/2 \tag{A18}$$

is the rate of incoherent dephasing caused by the repumping, and $\xi = \Gamma_1/\Gamma_2$.

Let us discuss briefly the light shifts Δ_j^{LS}. First, they are proportional to individual detunings Δ_j^p of the $|l\rangle \to |i\rangle$ pumping transition in the jth ion from the pumping field. These detunings depend on the micromotion-related second-order Doppler and Stark shifts. If the pumping field is tuned into resonance with the pumping transition of the ion in the center of the trap, they are proportional to $X_{j,0}^2 + Y_{j,0}^2$, as well as the micromotion-related shifts of the lasing transition (20), which may be compensated with the help of the fine tuning of the radio frequency Ω near its "magic" value Ω_0, as mentioned in the end of Sec. III. Third, light shifts are suppressed, in comparison with the detunings, by a factor of $(\xi+1)w/\Gamma$. For example, in the scheme with $^{176}\mathrm{Lu}^+$ ions considered in the paper, $\Gamma = 2.8\times10^7\ \mathrm{s}^{-1}$ and $\xi = 0.6$, which for $w \approx 100\ \mathrm{s}^{-1}$ gives $(\xi+1)w/\Gamma \approx 6\times10^{-6}$. In the present paper, we neglect this shift.

APPENDIX B: COUPLING OF ELECTRIC QUADRUPOLE TRANSITION WITH THE CAVITY FIELD

Here we suppose that the cavity mode is a Gaussian standing wave. For the sake of simplicity, we neglect the beam divergence and the Gouy phase; this simplification is valid, because we only need to calculate the coupling of the cavity mode with ions localized near the cavity waist. Then the electric field of the cavity mode is

$$\hat{\bar{E}}(\bar{r}) = \bar{e}\,\frac{\omega}{c}\sqrt{\frac{8\pi\hbar c^2}{V_{\mathrm{eff}}\,\omega}}\,e^{-\frac{r_\perp^2}{w_0^2}}\,\sin(\bar{k}\cdot\bar{r})[\hat{c}+\hat{c}^+], \tag{B1}$$

where $\bar{e}$ is the (complex) polarization unit vector, ω is the mode frequency, $\bar{k}$ is the wave vector, w_0 is the cavity waist, $V_{\mathrm{eff}} = \pi w_0^2 L$ is the effective mode volume, L is the cavity length, $\hat{c}$ is the (time-dependent) field operator, and $r_\perp = |\bar{r} - \bar{k}(\bar{k}\cdot\bar{r})/k^2|$ is the projection of $\bar{r}$ on the plane orthogonal to $\bar{k}$. The origin is on the axis of the cavity. If $w_0 \gg 1/k$, then the interaction of this electric field with quadrupole momentum $\hat{\mathcal{Q}}$ of some ion localized in the position $\bar{r}$ may be approximately written as

$$\hat{H}_{int} = \frac{1}{6}\frac{\partial\hat{E}_\alpha}{\partial x_\beta}\hat{\mathcal{Q}}_{\alpha\beta} \approx \frac{\mathrm{e}_\alpha k_\beta}{6}\hat{\mathcal{Q}}_{\alpha\beta}[\hat{c}+\hat{c}^+] \times\sqrt{\frac{8\pi\hbar\omega}{V_{\mathrm{eff}}}}\,\exp\left[-\frac{r_\perp^2}{w_0^2}\right]\cos(\bar{k}\cdot\bar{r}), \tag{B2}$$

where the summations over twice appearing Cartesian indices $\alpha,\beta,\ldots$ are implied here and below, for the sake of brevity. Cartesian components of the quadrupole momentum operator are

$$\hat{\mathcal{Q}}_{\alpha\beta} = \int(3x_\alpha x_\beta - \bar{r}^2\delta_{\alpha\beta})\hat{\rho}(\bar{r})d^3x, \tag{B3}$$

where $\hat{\rho}(\bar{r})$ is the operator of the charge density.

Let us consider some lasing transition between the upper and lower lasing states $|u\rangle$ and $|l\rangle$. Supposing that the ion is placed into the origin, we express the absolute value of the coupling strength $g(\bar{r})$ of the ion situated in $\bar{r}$ as

$$g(\bar{r}) = \frac{2}{\hbar}|\langle l,1|\hat{H}_{\mathrm{int}}|u,0\rangle| = g_0\,e^{-\frac{r_\perp^2}{w_0^2}}\cos(\bar{k}\cdot\bar{r}), \tag{B4}$$

where

$$g_0 = \sqrt{\frac{8\pi\omega}{\hbar\,V_{\mathrm{eff}}}}\left|\frac{e_\alpha k_\beta}{3}\langle l|\hat{\mathcal{Q}}_{\alpha\beta}|u\rangle\right| \tag{B5}$$

is the coupling coefficient for the ion placed on the cavity axis in the antinode of the mode.

The quadrupole momentum $\hat{\mathcal{Q}}$ is the symmetric traceless second-rank tensor, and its Cartesian components may be expressed via the spherical components

$$\hat{\mathcal{Q}}_{2q} = \sqrt{\frac{4\pi}{5}}\int r^2\hat{\rho}(\bar{r})Y_{2q}\left(\frac{\bar{r}}{r}\right)d^3x \tag{B6}$$

as

$$\hat{\mathcal{Q}}_{xx} = \sqrt{\frac{3}{2}}(\hat{\mathcal{Q}}_{22}+\hat{\mathcal{Q}}_{2-2}) - \hat{\mathcal{Q}}_{20}, \tag{B7}$$

$$\hat{\mathcal{Q}}_{yy} = -\sqrt{\frac{3}{2}}(\hat{\mathcal{Q}}_{22}+\hat{\mathcal{Q}}_{2-2}) - \hat{\mathcal{Q}}_{20}, \tag{B8}$$

$$\hat{\mathcal{Q}}_{zz} = 2\hat{\mathcal{Q}}_{20}, \tag{B9}$$

$$\hat{\mathcal{Q}}_{xy} = -i\sqrt{\frac{3}{2}}(\hat{\mathcal{Q}}_{22}-\hat{\mathcal{Q}}_{2-2}), \tag{B10}$$

$$\hat{\mathcal{Q}}_{zx} = \sqrt{\frac{3}{2}}(\hat{\mathcal{Q}}_{21}-\hat{\mathcal{Q}}_{2-1}), \tag{B11}$$

$$\hat{\mathcal{Q}}_{zy} = -i\sqrt{\frac{3}{2}}(\hat{\mathcal{Q}}_{21}+\hat{\mathcal{Q}}_{2-1}). \tag{B12}$$

Now we should express the matrix elements of $\hat{\mathcal{Q}}_{2q}$ via the rate γ of spontaneous transition. The states $|a\rangle = |\eta_a J_a I F_a m_a\rangle$ ($a = u$ or l) are characterized by principal quantum numbers η_a, the electronic shell angular momenta J_a, the nuclear angular momentum I, the total angular momenta F_a, and its projections m_a. Then, according to the well-known expression for the electric multipole spontaneous transition rate [34] we can write

$$\gamma = \frac{\omega^5}{15\hbar c^5}\sum_{F_l,m_l}|\langle\eta_u J_u I F_u m_u|\hat{\mathcal{Q}}_{2q}|\eta_l J_l I F_l m_l\rangle|^2. \tag{B13}$$

Using the Wigner-Eckart theorem [35], we can express the matrix element as

$$\langle\eta_u J_u I F_u m_u|\hat{\mathcal{Q}}_{2q}|\eta_l J_l I F_l m_l\rangle = (-1)^{F_l+J_u+I-2}\sqrt{2F_l+1}\,C_{F_l m_l 2q}^{F_u m_u} \times\begin{Bmatrix} J_l & I & F_l \\ F_u & 2 & J_u\end{Bmatrix}\langle\eta_u J_u||\hat{\mathcal{Q}}_2||\eta_l J_l\rangle, \tag{B14}$$

where $\langle \eta_u J_u || \hat{\mathcal{Q}}_2 || \eta_l J_l \rangle$ is a reduced matrix element. Using the properties of the Clebsch-Gordan coefficients and $6J$ symbols [35]

$$\sum_{m_l,q} \left(C^{F_u m_u}_{F_l m_l 2q}\right)^2 = 1, \tag{B15}$$

$$\sum_{F_l} (2F_l+1) \begin{Bmatrix} J_l & I & F_l \\ F_u & 2 & J_u \end{Bmatrix}^2 = \frac{1}{2J_u+1}, \tag{B16}$$

we obtain

$$\langle \eta_u J_u || \hat{\mathcal{Q}}_2 || \eta_l J_l \rangle^2 = \frac{15\hbar c^5 \gamma (2J_u+1)}{\omega^5}, \tag{B17}$$

which gives

$$\begin{aligned} &\langle \eta_u J_u I F_u m_u | \hat{\mathcal{Q}}_{2q} | \eta_l J_l I F_l m_l \rangle^2 \\ &= (2F_l+1)(2J_u+1) \left(C^{F_u m_u}_{F_l m_l 2q}\right)^2 \\ &\times \begin{Bmatrix} J_l & I & F_l \\ F_u & 2 & J_u \end{Bmatrix}^2 \frac{15\hbar c^5 \gamma}{\omega^5}. \end{aligned} \tag{B18}$$

Let us calculate the coupling strengths g for the circularly polarized cavity mode in the configuration shown in Fig. 1, i.e., when $\bar{e} = (i\bar{e}_y \pm \bar{e}_x)/\sqrt{2}$ and $\bar{k} = \bar{e}_z \omega/c$. Then

$$e_\alpha k_\beta \hat{\mathcal{Q}}_{\alpha\beta} = \frac{\omega}{c\sqrt{2}} (i\hat{\mathcal{Q}}_{yz} \pm \hat{\mathcal{Q}}_{xz}) = \frac{\omega\sqrt{3}}{c} \hat{\mathcal{Q}}_{2\pm 1}. \tag{B19}$$

Substituting Eq. (B19) into Eq. (B5), we obtain

$$g_0 = \frac{\omega}{c\sqrt{3}} \sqrt{\frac{8\pi\omega}{\hbar V_{\text{eff}}}} \langle l | \hat{\mathcal{Q}}_{2\pm 1} | u \rangle. \tag{B20}$$

One can see that transitions with $m_u - m_l = \pm 1$ can be coupled with the cavity mode in such a configuration.

Let us suppose, for the sake of definiteness, that $m_u = m_l$. Then

$$\begin{aligned} g_0^2 &= \frac{40\pi c^3 \gamma}{V_{\text{eff}}\, \omega^2} (2F_l+1)(2J_u+1) \\ &\times \begin{Bmatrix} J_l & I & F_l \\ F_u & 2 & J_u \end{Bmatrix}^2 \left(C^{F_u m_u}_{F_l m_l 2\pm 1}\right)^2 = \frac{5\pi c^3 \gamma}{V_{\text{eff}}\, \omega^2} \Theta^2_{ul}, \end{aligned} \tag{B21}$$

where Θ^2_{ul} is given by Eq. (38).

APPENDIX C: HYPERFINE STRUCTURE OF $^{176}Lu^+$ $^3D_2$ STATE AND SECOND-ORDER ZEEMAN SHIFT

The hyperfine structure of low-lying levels of $^{175}Lu^+$ ions ($I = 7/2$) was measured in Ref. [36]. In particular, it was found that the energies of the hyperfine sublevels of the $^3D_2$ state grow as F increases from 3/2 to 11/2. The distances between adjacent levels are 0.139, 0.210, 0.288, and 0.382 cm^{-1}. Using the standard expression for the hyperfine energy levels

$$\begin{aligned} \frac{E_{\text{hfs}}(F)}{\hbar} &= A_{\text{hfs}} \frac{K}{2} \\ &+ B_{\text{hfs}} \frac{\frac{3}{2}K(K+1) - 2I(I+1)J(J+1)}{4I(2I-1)J(2J-1)} \end{aligned} \tag{C1}$$

where

$$K = F(F+1) - J(J+1) - I(I+1), \tag{C2}$$

we can fit the hyperfine constants as $A_{\text{hfs},175} = 2\pi \times 1935$ MHz, $B_{\text{hfs},175} = 2\pi \times 1388$ MHz.

To estimate the hyperfine constants $A_{\text{hfs},176}$ and $B_{\text{hfs},176}$ for the $^3D_2$ state of the $^{176}Lu^+$ ion, we can use the fact that B_{hfs} is proportional to the nuclear quadrupole moment, and A_{hfs} is proportional to the nuclear g factor $g_I = -\mu/(I\mu_B)$, where μ is the nuclear magnetic moment and μ_B is the Bohr magneton.

According to Ref. [37], nuclear quadrupole moments of $^{175}Lu^+$ and $^{176}Lu^+$ are 3415 and 4818 mb, respectively, which gives $B_{\text{hfs},176} = 2\pi \times 1963$ MHz. In turn, the magnetic moments are $\mu_{175} = 2.2327\mu_N$ and $\mu_{176} = 3.162\mu_N$ according to Ref. [38], which gives $A_{\text{hfs},176} = 2\pi \times 1370$ MHz.

In the presence of external magnetic field $\bar{B}$, the hyperfine energy levels experience a Zeeman splitting. Magnitudes of the Zeeman shift may be found from the diagonalization of the hyperfine-Zeeman Hamiltonian

$$\begin{aligned} \frac{\hat{H}}{\hbar} &= \mu_B (g_I \hat{\bar{I}} + g_J \hat{\bar{J}}) \cdot \bar{B} + A_{\text{hfs}} \hat{\bar{I}} \cdot \hat{\bar{J}} \\ &+ \frac{3B_{\text{hfs}}}{4J(2J-1)I(2I-1)} \\ &\times \left[2(\hat{\bar{I}} \cdot \hat{\bar{J}})^2 + \hat{\bar{I}} \cdot \hat{\bar{J}} - \frac{2}{3} \hat{\bar{I}}^2 \hat{\bar{J}}^2 \right], \end{aligned} \tag{C3}$$

where

$$\begin{aligned} g_J &= g_L \frac{J(J+1) - S(S+1) + L(L+1)}{2J(J+1)} \\ &+ g_S \frac{J(J+1) + S(S+1) - L(L+1)}{2J(J+1)} \end{aligned} \tag{C4}$$

is the electronic Lande g factor. Taking $g_L = 1$, $g_S = 2.002319043617$, $L = 2$, $S = 1$, and $J = 2$, we find $g_J \approx 1.16705$. Also, $g_I \approx -0.000246$ for $^{176}Lu^+$.

In weak magnetic field $\bar{B}$ the Zeeman shifts $\Delta_{Z|F,m_F=0\rangle}(B)$ of the states $|F, m_F = 0\rangle$ are quadratic in $|\bar{B}|$. We find

$$\begin{aligned} &\frac{\Delta_{Z|5,0\rangle}(B)}{2\pi |\bar{B}|^2} = -440.0 \frac{\text{Hz}}{\text{G}^2}, \quad \frac{\Delta_{Z|6,0\rangle}(B)}{2\pi |\bar{B}|^2} = -15.19 \frac{\text{Hz}}{\text{G}^2}, \\ &\frac{\Delta_{Z|7,0\rangle}(B)}{2\pi |\bar{B}|^2} = 127.3 \frac{\text{Hz}}{\text{G}^2}, \quad \frac{\Delta_{Z|8,0\rangle}(B)}{2\pi |\bar{B}|^2} = 166.3 \frac{\text{Hz}}{\text{G}^2}, \\ &\frac{\Delta_{Z|9,0\rangle}(B)}{2\pi |\bar{B}|^2} = 165.5 \frac{\text{Hz}}{\text{G}^2}. \end{aligned} \tag{C5}$$

In turn, the Zeeman shift $\Delta_{Z,0}$ of the state $|^1S_0, m = 1\rangle$ (playing the role of the lower lasing state in the scheme considered in the main text) is determined by the nuclear gyromagnetic ratio and is linear in the magnetic field: $\Delta_{Z,0}/B_z = -2\pi \times 344.3$ Hz/G.

The "magic" value B_m of the magnetic field is such a value of the z projection of this field that the frequency difference between the upper and the lower clock states (or lasing states in our case) are insensitive in the leading order to the fluctuations of this field. Magic fields can be easily found for various transitions from the equating of the first derivatives of the Zeeman shifts of the upper and the lower lasing states.

[1] B. J. Bloom, T. L. Nicholson, J. R. Williams, S. L. Campbell, M. Bishof, X. Zhang, W. Zhang, S. L. Bromley, and J. Ye, Nature (London) **506**, 71 (2014).

[2] N. Huntemann, C. Sanner, B. Lipphardt, Chr. Tamm, and E. Peik, Phys. Rev. Lett. **116**, 063001 (2016).

[3] R. M. Godun, P. B. R. Nisbet-Jones, J. M. Jones, S. A. King, L. A. M. Johnson, H. S. Margolis, K. Szymaniec, S. N. Lea, K. Bongs, and P. Gill, Phys. Rev. Lett. **113**, 210801 (2014).

[4] C. W. Chou, D. B. Hume, T. Rosenband, and D. J. Wineland, Science **329**, 1630 (2010).

[5] C. Audoin, G. Santarelli, A. Makdissi, and A. Clarion, IEEE Trans. Ultrason. Ferroel. Freq. Control **45**, 877 (1998).

[6] K. Numata, A. Kemery, and J. Camp, Phys. Rev. Lett. **93**, 250602 (2004).

[7] S. Häfner, S. Falke, Chr. Grebing, S. Vogt, T. Legero, M. Merimaa, Chr. Lisdat, and U. Sterr, Opt. Lett. **40**, 2112 (2015).

[8] D. G. Matei, T. Legero, S. Häfner, C. Grebing, R. Weyrich, W. Zhang, L. Sonderhouse, J. M. Robinson, J. Ye, F. Riehle, and U. Sterr, Phys. Rev. Lett. **118**, 263202 (2017).

[9] J. Chen and X. Chen, in *Proceedings of the 2005 IEEE International Frequency Control Symposium and Exposition* (IEEE, New York, 2005), pp. 608–610.

[10] D. Meiser, J. Ye, D. R. Carlson, and M. J. Holland, Phys. Rev. Lett. **102**, 163601 (2009).

[11] D. Yu and J. Chen, Phys. Rev. A **78**, 013846 (2008).

[12] J. G. Bohnet, Z. Chen, J. M. Weiner, D. Meiser, M. J. Holland, and James K. Thompson, Nat. Lett. **484**, 78 (2012).

[13] K. C. Cox, J. M. Weiner, and James K. Thompson, Phys. Rev. A **90**, 053845 (2014).

[14] J. M. Weiner, K. C. Cox, J. G. Bohnet, and J. K. Thompson, Phys. Rev. A **95**, 033808 (2017).

[15] M. A. Norcia and J. K. Thompson, Phys. Rev. X **6**, 011025 (2016).

[16] M. A. Norcia, M. N. Winchester, J. R. K. Cline, and J. K. Thompson, Sci. Adv. **2**, e1601231 (2016).

[17] A. Derevianko and H. Katori, Rev. Mod. Phys. **83**, 331 (2011).

[18] G. A. Kazakov and T. Schumm, Phys. Rev. A **87**, 013821 (2013).

[19] G. Kazakov and T. Schumm, Proc. EFTF **2014**, 411 (2014).

[20] F. Schreck (private communication).

[21] P. Bowe, L. Hornekær, C. Brodersen, M. Drewsen, J. S. Hangst, and J. P. Schiffer, Phys. Rev. Lett. **82**, 2071 (1999).

[22] J. Keller, T. Burgermeister, D. Kalincev, J. Kiethe, and T. E. Mehlstäubler, J. Phys.: Conf. Ser. **723**, 012027 (2016).

[23] K. Arnold, E. Hajiyev, E. Paez, C. H. Lee, M. D. Barrett, and J. Bollinger, Phys. Rev. A **92**, 032108 (2015).

[24] G. A. Kazakov and T. Schumm, Phys. Rev. A **95**, 023839 (2017).

[25] H. Landa, M. Drewsen, B. Reznik, and A. Retzker, New J. Phys. **14**, 093023 (2012).

[26] W. M. Itano, J. Res. Natl. Inst. Stand. Technol. **105**, 829 (2000).

[27] E. Paez, K. J. Arnold, E. Hajiyev, S. G. Porsev, V. A. Dzuba, U. I. Safronova, M. S. Safronova, and M. D. Barrett, Phys. Rev. A **93**, 042112 (2016).

[28] M. Xu, D. A. Tieri, E. C. Fine, J. K. Thompson, and M. J. Holland, Phys. Rev. Lett. **113**, 154101 (2014).

[29] M. J. Martin, D. Meiser, J. W. Thomsen, Jun Ye, and M. J. Holland, Phys. Rev. A **84**, 063813 (2011).

[30] P. G. Westergaard, B. T. R. Christensen, D. Tieri, R. Matin, J. Cooper, M. Holland, J. Ye, and J. W. Thomsen, Phys. Rev. Lett. **114**, 093002 (2015).

[31] K. J. Arnold and M. D. Barrett, Phys. Rev. Lett. **117**, 160802 (2016).

[32] T. Maier, S. Kraemer, L. Ostermann, and H. Ritsch, Opt. Express **22**, 13269 (2014).

[33] S. Krämer and H. Ritsch, Eur. Phys. J. D **69**, 282 (2015).

[34] V. B. Berestetskii, E. M. Lifshitz, and L. P. Pitaevskii, *Quantum Electrodynamics*, Course of Theoretical Physics Vol. 4 (Pergamon Press, New York, 1982).

[35] D. A. Varshalovich, A. N. Moskalev, and V. K. Khersonskii, *Quantum Theory of Angular Momentum* (World Scientific, Singapore, 1988).

[36] H. H. Schüler and Th. Schmidt, Z. Phys. **95**, 265 (1935).

[37] R. L. A. Haiduke, A. B. F. da Silva, and L. Visscher, Chem. Phys. Lett. **445**, 95 (2007).

[38] N. J. Stone, At. Data Nucl. Data Tables **90**, 75 (2005).